STAR Note #223
November 12, 1995

Reconstructing the Parameters of Charged Particle Hits in the SDD

V. L. Rykov[1]

For the STAR SVT Collaboration

Department of Physics and Astronomy
Wayne State University
Detroit, MI 48201

Abstract

The performance of the STAR Silicon Vertex Tracker and its dependence on signal shaping, noise, readout characteristics, and data processing algorithms are discussed. The position and charge resolutions are evaluated. The results have been obtained by Monte-Carlo simulations.

[1]Visitor from IHEP, Protvino, Moscow District 142284, Russia

1 Introduction

The performance of the Silicon Drift Detector (SDD) [1], the basic unit of the STAR Silicon Vertex Tracker (SVT) [2], depends on many factors. Among the most important of them is the appropriate SDD signal processing at the lowest hardware and software levels. In this paper, the dependence of the SDD performance on the detector and Preamplifier-Shaper (PASA) characteristics, noise level, and data processing algorithms is discussed.

SDD signals have been evaluated using *SDD_SIGNAL* codes [3][2] based on a recently developed approach [4, 5] to the electron cloud's expansion dynamics during its drift in the SDD, taking into account an electron diffusion and Coulomb repulsion. In these simulations the SDD was assumed to have the following parameters:

Silicon diffusion constant	D	$= 3.5 \cdot 10^{-3}\, mm^2/\mu s$;
Electron mobility in Silicon	μ	$= 0.135\, mm^2/V \cdot \mu s$;
Silicon dielectric constant	ε	$= 12$;
Silicon ionization energy	E_{pair}	$= 3.6\, eV/pair$;
SDD thickness	d	$= 0.3\, mm$;
SDD size (Anode×Drift)	$Z_{max} \times X_{max}$	$= 60 \times 30\, mm^2$;
Anode pitch size (anode width + gap)	Δ_z	$= 0.25\, mm$;
Number of anodes/SDD (number of channels)	N_{anode}	$= 240$.

In most of the results presented here, the SDD bias (drift voltage) U has been set to $1428\, V$ unless a different voltage is mentioned explicitly. This corresponds to an electron drift velocity $V_{drift} = 6.43\, mm/\mu s$ with a maximum drift time $t_{max} = X_{max}/V_{drift} = 4.67\, \mu s$.

It has been assumed that the electron cloud in the SDD middle plane has a two dimensional Gaussian shape, and that the cloud expansion dynamics during its drift are governed by the equations from references [4, 5]. The time dependence of the anode current has also been approximated by a Gaussian. The signal widening of ~6 ns due to the electrostatic charge induced at the anodes by the approaching electron cloud has been taken into account as well.

The impact of the PASA on the signal shape is determined by the PASA transformation function, $f_{pasa}(t)$, the PASA response to the input current $i(t) = e \cdot \delta(t)$, where e is the charge of a single electron. In the present SVT PASA design, the Laplace representation for $f_{pasa}(t)$ is the following [6, 7]:

$$F_{pasa}(s) \propto \frac{s}{(s + 1/\tau_s)^n (s + 1/\tau_l)}$$

with $n = 5$. Two PASA options with different sets of time-constants $\tau_{s,l}$ are compared:

PASA$_{short}$: $\tau_s = 11.5\, ns$ $\tau_l = 500\, ns$ (current design)

PASA$_{long}$: $\tau_s = 18.0\, ns$ $\tau_l = 750\, ns$

The PASA gain, G_{pasa}, has been chosen such that $G_{pasa} \equiv max\{f_{pasa}(t)\} = 9.5\, \mu V/e$. The transformation functions for PASA$_{short}$ and PASA$_{long}$ are shown in Fig. 1. The FWHM of the positive peak, W_{pasa}, is ≃52 ns for PASA$_{short}$ and ≃80 ns for PASA$_{long}$. The positions of the $f(t)$ maximum (peaking time) are at t_{peak} ≃45 and 70 ns for PASA$_{short}$ and PASA$_{long}$, respectively.

[2]The codes are available in STAR TAS, thanks to C. Pruneau and D. Read.

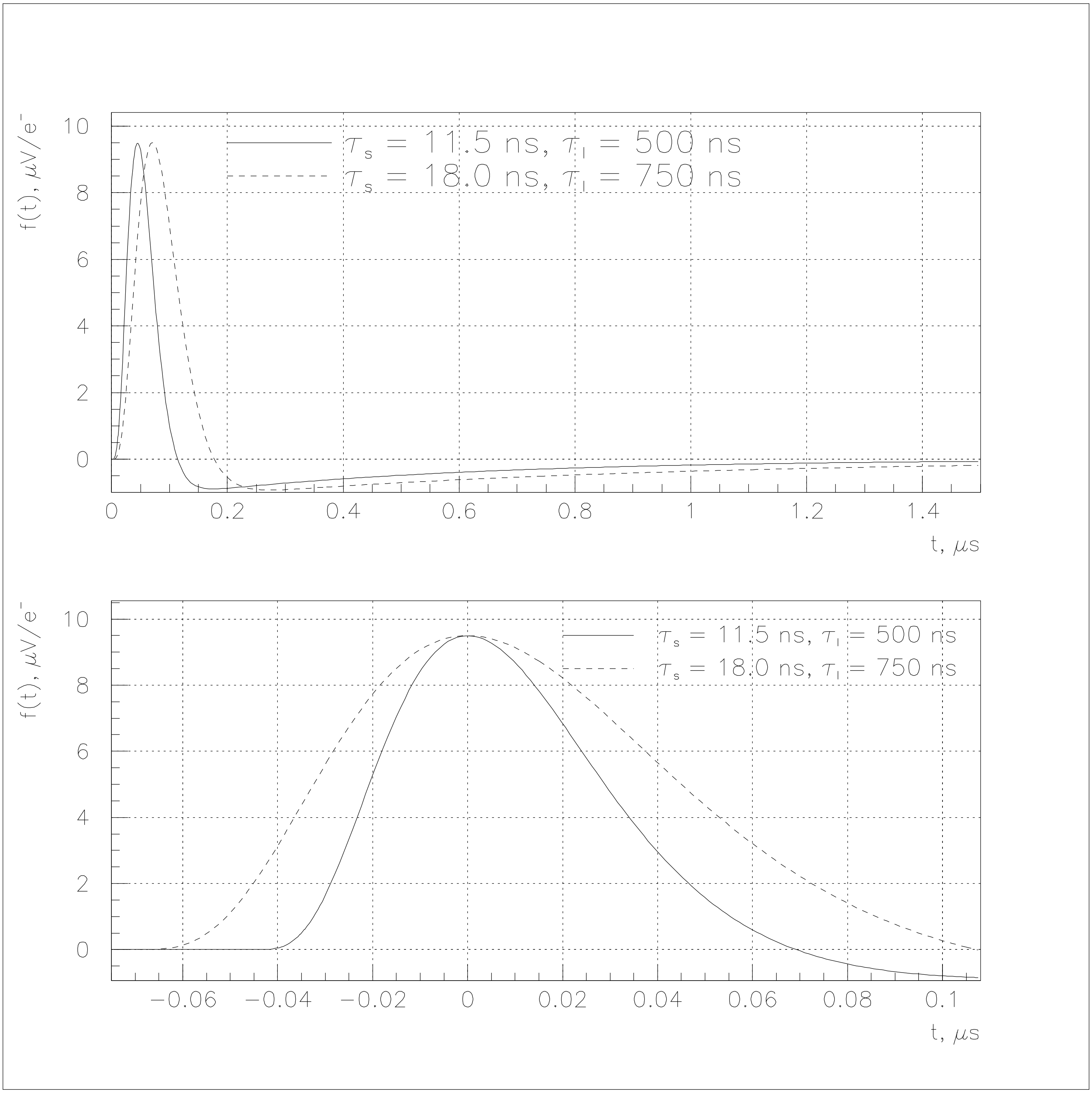

Figure 1: PASA transformation functions (two different time scales).

Signal fluctuations due to electronics noise have been simulated using the *CORR_NOISE* code [8][3] . Throughout this paper, if not mentioned explicitly, it has been assumed that there is a "white noise" at the PASA input, which is then transformed with the PASA transformation function $f_{pasa}(t)$, creating correlated noise at the PASA output. Landau fluctuations of the particle ionization losses, normalized to the experimental data [9], have also been taken into account.

2 Data taking and processing chain

The following is a summary of the STAR SVT data taking and processing chain[2]. After receiving the lowest level trigger, the signals from the PASA outputs, for each channel, are measured N_{time} times at a frequency f_{SCA} during the drift time of the ionization in the SDD. The results of the measurements are stored in Switch Capacitor Arrays (SCAs). The measurement time is ~1–3 $ns \ll \tau_s \simeq$12–18 ns. Thus, the analog data stored in the SCA are, in fact, instantaneous voltages at the PASA outputs at the time of measurement. The analog data are digitized by 10-bit ADCs and then read out by the Data Acquisition System (DAQ). The ADC effective dynamic range for the signals will be ~2–2.1 V with a resolution ~2.15 mV/count [7, 10].

For most of the simulations discussed in this note, the SCA sampling frequency f_{SCA} (SCA clock) has been set to 26.77 MHz. That implies that no more than $N_{time} = 128$ time slices need to be taken to cover the maximum drift time $t_{max} = 4.67\,\mu s$. For V_{drift} and f_{SCA} above, the space sampling period in the drift direction, $\Delta_x = V_{drift}/f_{SCA} \simeq 0.24\,mm$, is about the same as the sampling along the anodes, $\Delta_z = 0.25\,mm$.

The data are transfered from the ADCs using specially designed custom chips, ASICs, which take digitized signals from the ADCs and store them in the DAQ memory buffers as two-dimensional arrays of signals u_{ij} of size $N_{anode} \times N_{time}$ for each SDD. At data taking time the ASIC performs also the following operations:

- Pedestal subtraction;
- Nonlinear compression of the original 10 bit ADC data to 8 bits;
- Recognition of the "nonzero" signals for each channel as a sequence of time-pixels above some threshold(s) and building a so called "cluster guide" which points to the time-clusters which were found.

After the ASIC operation is completed, data are available for processing by the front-end DAQ processors located at the readout boards. At this stage, various calculations will be performed: building two-dimensional clusters corresponding to potential particle hits, calculation of the moments of 2D-clusters and of some other characteristics for further usage in the high level (software) trigger, downloading the "approved" events into the Event Builder, and so on.

In the next sections, we discuss the impact of various factors in the data processing chain on the SVT performance, trying to separate the contribution of each factor from the others whenever possible.

[3]The codes are available in STAR TAS, thanks to D. Read.

3 2D-cluster

2D-clusters, representing particle hits, can be defined, in general, as contiguous two-dimensional sets of pixels u_{ij} surrounding the "centers of the clusters", usually the pixels with the highest signal in a local area. This definition does not spell out, however, the criteria for any particular pixel to be included in the cluster, which will undoubtedly affect the SDD performance. For example, if a 2D-cluster contains too few pixels, the accuracy of the reconstruction of the particle hit parameters may be significantly worse than the setup is capable of providing. On the other hand, if "for safety" the acquired clusters are too large, there is an unnecessary overhead in the required DAQ and data processing resources (memory, bandwidth, etc), while the reconstruction accuracy may not be improved. Moreover, due to the high multiplicity of charged particles expected in heavy ion collisions at RHIC, the probability for large clusters to merge increases, complicating the data analysis.

The right choice of the exact 2D-cluster definition depends on many factors, such as the signal-to-noise ratio and selection criteria of the "zero-suppression/cluster-finder" algorithm. A detailed consideration of zero-suppression/cluster-finder algorithms is out of the scope of this paper. Here we define 2D-clusters as contiguous sets of undisturbed (i.e. without noise) pixels u_{ij} above a certain threshold u_{min}. The noise is then added on top of the signals within a 2D-cluster without changing its boundaries.

A threshold u_{min}, or in terms of collected charge $q_{min} = u_{min}/G_{pasa}$ is, again, the subject for an optimization in the zero-suppression algorithm, which is not discussed here. In this paper, the results of simulations are usually provided for q_{min} equal to $1 \cdot ENC$ and $5 \cdot ENC$, where ENC is an equivalent noise charge. The SDD performance estimates at the lower threshold should be considered as being rather optimistic, but $q_{min} = 5 \cdot ENC$ ("pessimistic" estimates) should be certainly high enough to reject false clusters due to noise, down to a level of $\leq$0.1 false cluster/event per SDD. This corresponds to $\leq$0.5–1% of the track density for the central Au-Au event, and to $\leq$5–10% for pp collisions at the luminosity of $2 \cdot 10^{32}\, cm^{-2} s^{-1}$.

4 SDD signals and 2D-cluster size

In Fig. 2, the signals without noise at the "central" anode are shown for two ionization levels and various drift distances. The ionization of $25,000e$ is about the most probable for a "minimum ionizing particle" (MIP). The level of $750,000$ corresponds to the ionization from a "slow proton" with the momentum of $\sim$150 MeV/c. The signal amplitude variations vs drift distance X are shown in Fig. 3. The variation of the signal at the central anode for a fixed hit position Z along the anode axis and for a fixed ionization, is about 3 – 3.5 times for a MIP due to electron cloud expansion during its drift. It is even higher, 6 – 8 times, for high ionizing particles. For PASA$_{long}$, the variation is smaller than for PASA$_{short}$.

The actual variation of the measured signals in the 2D-clusters originating from particle hits is even larger due to fluctuations of the created ionization, the random positions of the particle hits relative to the nearest anode center, and noise from the electronics. Fig. 4a illustrates this type of distribution for a MIP crossing the SDD at $X = 15\, mm \pm \Delta_x/2$. One can observe that, while the largest signals in the two adjacent channels are on the order of tens of mV, the signal in the third channel sometimes drops to a few mV. This means

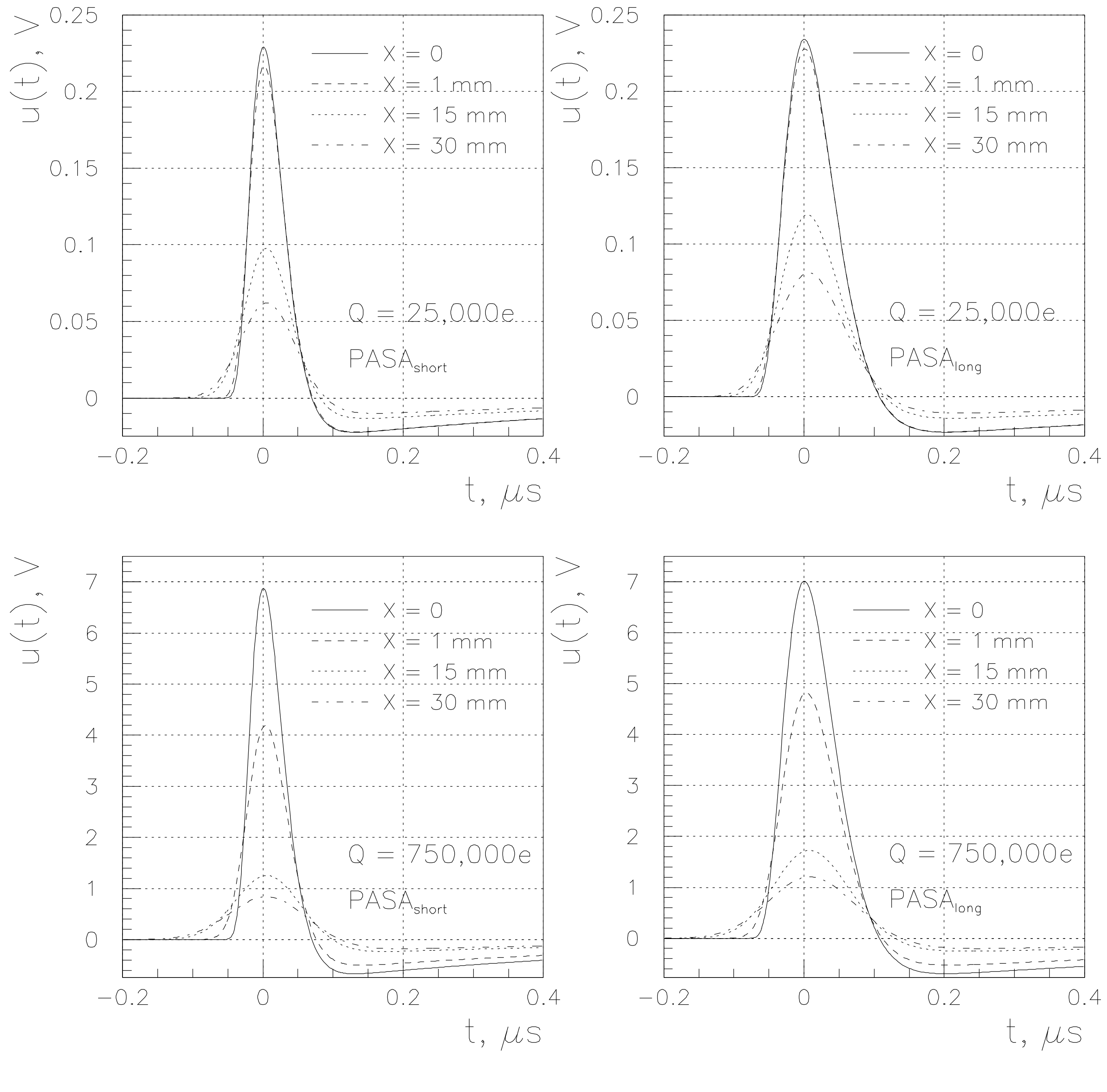

Figure 2: SDD signals at the central anode for various drift distances X. Perpendicular particle hits are directly in front of the anode center.

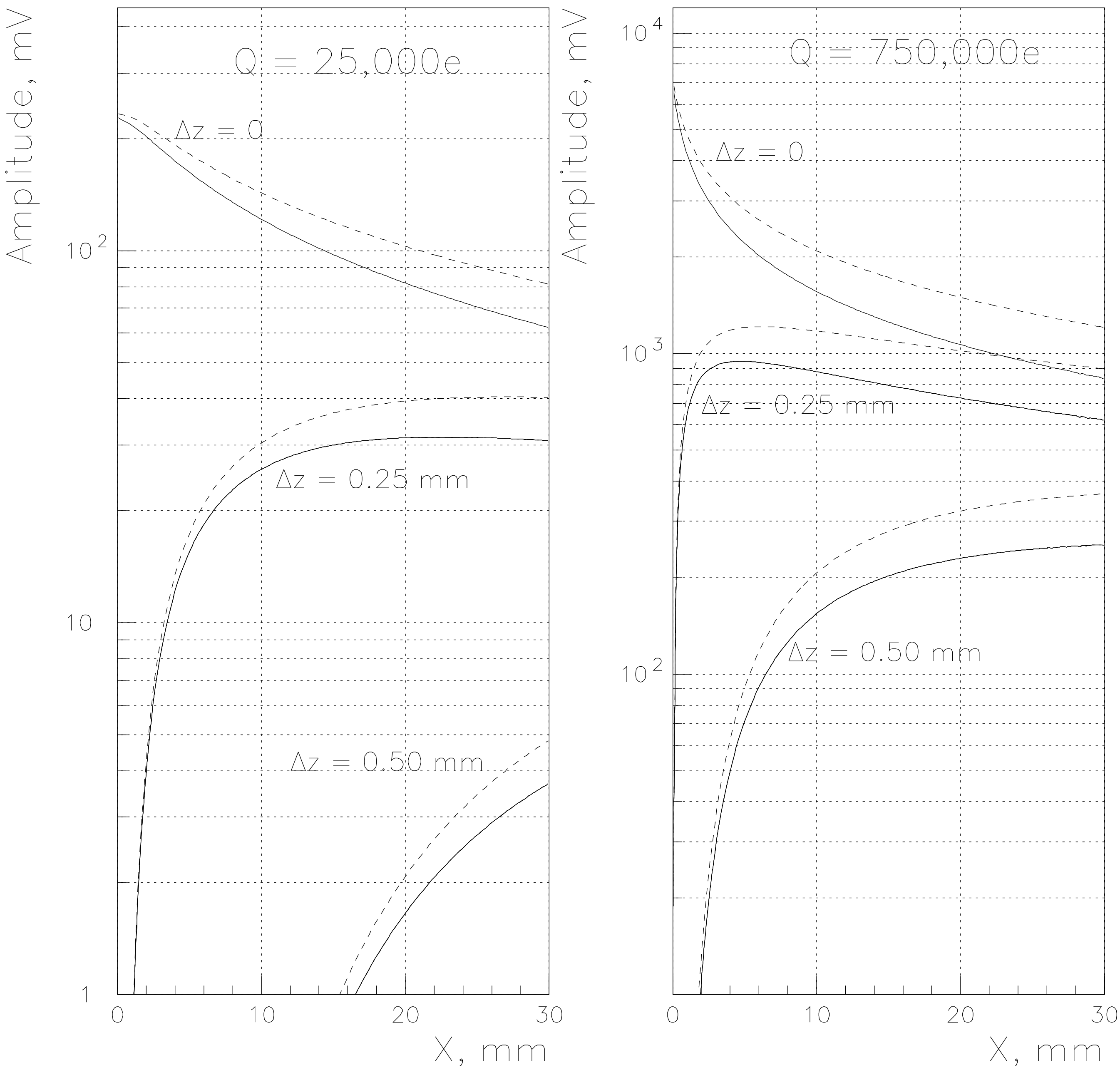

Figure 3: Signal amplitude vs drift distance X for perpendicular particle hits. Solid lines are for PASA$_{short}$ and dashed lines are for PASA$_{long}$. The distance Δz is the displacement of the particle hit from the anode center.

that some MIP hits in the mid-SDD will have no more than 2 anodes with signals above even a quite low threshold of u_{min} ~5–10 mV which is equivalent to q_{min} ~500–1,000e. The distributions of 2D-cluster sizes in both the anode and the drift directions for the same hits are shown in Fig. 4b and c. The dependencies of the mean cluster widths vs drift distance for $q_{min} = 400$ and $2000e$ are presented in Fig. 5. While the number of anodes in a 2D-cluster is almost independent of the PASA shaping time, the clusters are significantly wider in the drift direction for PASA$_{long}$, and even for the high threshold of $q_{min} = 2000e$, the mean value of the time-width is never less than 4 time slices.

The cluster size by itself does not determine directly any characteristic of the SDD performance. However, if the cluster size is too small, some reconstruction algorithms will not work. For example, a Gaussian or any other three-parameter fit (charge, centroid and width) to the signal distribution in any direction requires a minimum 2D-cluster width of three anodes or time slices. Moreover, if the cluster width is just about one anode, as is the case for short drifts $X \leq$1–2 mm, one should not expect the position resolution to be significantly different from $\Delta_z/\sqrt{12} \simeq 70\,\mu m$. On the other hand, if the cluster gets too wide, i.e. the ionization charge is spread over many pixels, then the position resolution will worsen again due to the lowering of the signal-to-noise ratio for each individual pixel. The double particle resolution, which is important for HBT measurements, may also be degraded if the cluster width is increased.

5 Reconstruction of the particle hit parameters

In this section, three common approaches for the reconstruction of 2D-cluster parameters are compared.

5.1 Moment analysis

The basis of the "Moment analysis" algorithm is the calculation of the moments of the signal distribution over 2D-cluster. The electron cloud charge Q_M can be expressed using the 0-th moment $\mathcal{M}_0 = \sum_{i,j} u_{ij}$:

$$Q_M \simeq \frac{2.355\,\Delta_x}{\sqrt{2\pi}\,G_{pasa}\,W_{pasa}\,V_{drift}} \sum_{i,j} u_{ij} \quad , \quad u_{ij} \geq u_{min} \quad , \tag{1}$$

where u_{ij} is the signal in the i-th channel measured at the time moment t_j, corresponding to the j-th time-slice, and u_{min} is the threshold of the zero-suppression algorithm. The particle hit coordinates can be determined using the 1-st moments of the same distribution:

$$Z_M \equiv m_1 \equiv \frac{\mathcal{M}_1}{\mathcal{M}_0} = \frac{\sum_{i,j} Z_i \cdot u_{ij}}{\sum_{i,j} u_{ij}} \; ; \; X_M \equiv m_2 \equiv \frac{\mathcal{M}_2}{\mathcal{M}_0} = \frac{\sum_{i,j} V_{drift} \cdot t_j \cdot u_{ij}}{\sum_{i,j} u_{i,j}}, \tag{2}$$

where Z_i is the position of the center of the i-th anode.

The 2-nd moments,

$$m_{11} = \frac{\sum_{i,j} Z_i^2 u_{ij}}{\mathcal{M}_0} - m_1^2 \; ; \; m_{22} = V_{drift}^2 \frac{\sum_{i,j} t_j^2 u_{ij}}{\mathcal{M}_0} - m_2^2 \; ; \; m_{12} = V_{drift} \frac{\sum_{i,j} Z_i\, t_j u_{ij}}{\mathcal{M}_0} - m_1 m_2 \;\; ,$$

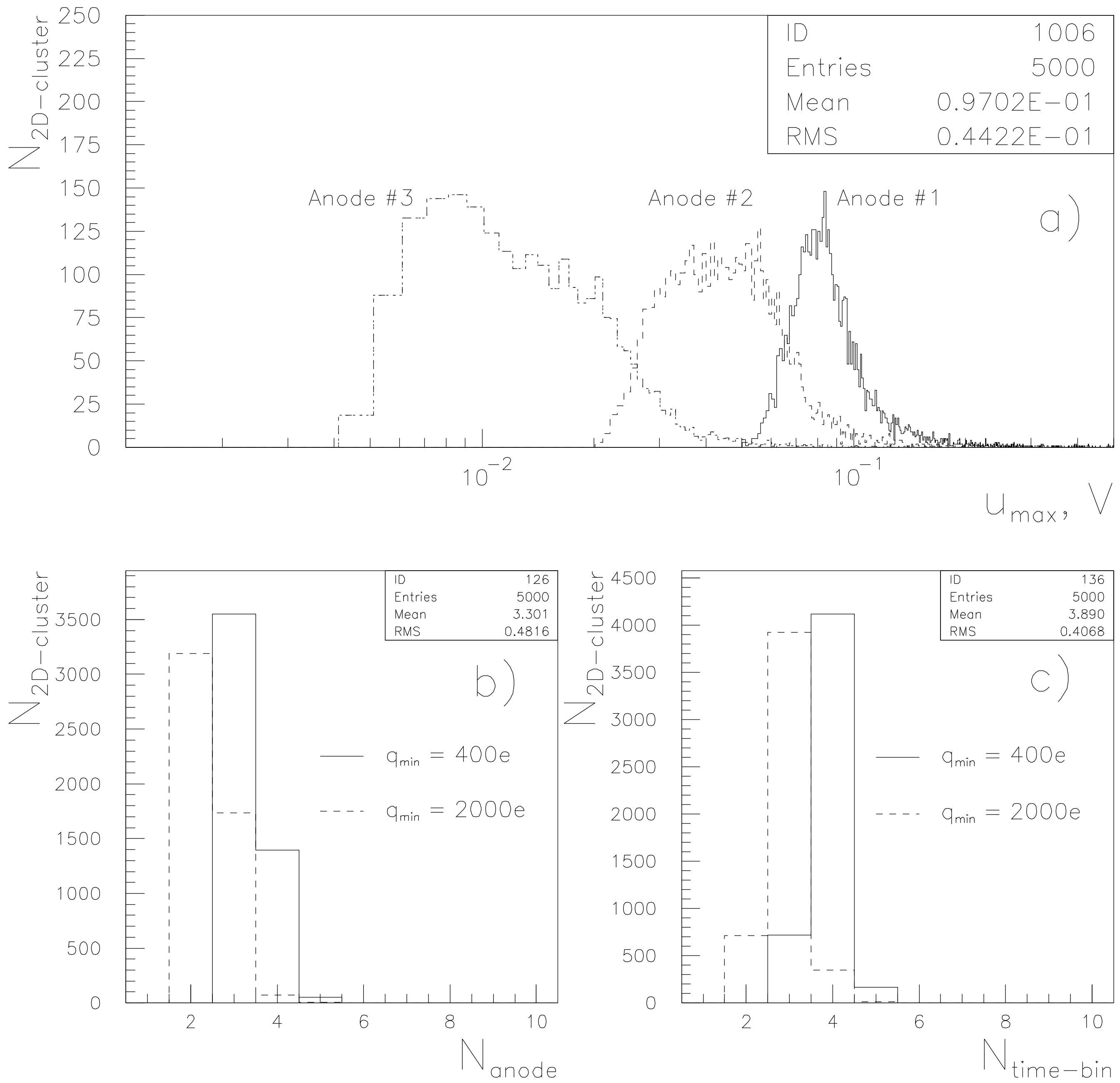

Figure 4: MIP, perpendicular hit, $X = 15\,mm$, PASA$_{short}$, no noise: **a)** - The highest amplitudes in three adjacent anodes (the histogram statistics are for Anode #1). Number of anodes, **b)**, and time slices, **c)**, per 2D-cluster with at least one pixel above $u_{min} = G_{pasa} \cdot q_{min}$ (the histogram statistics correspond $q_{min} = 400e$).

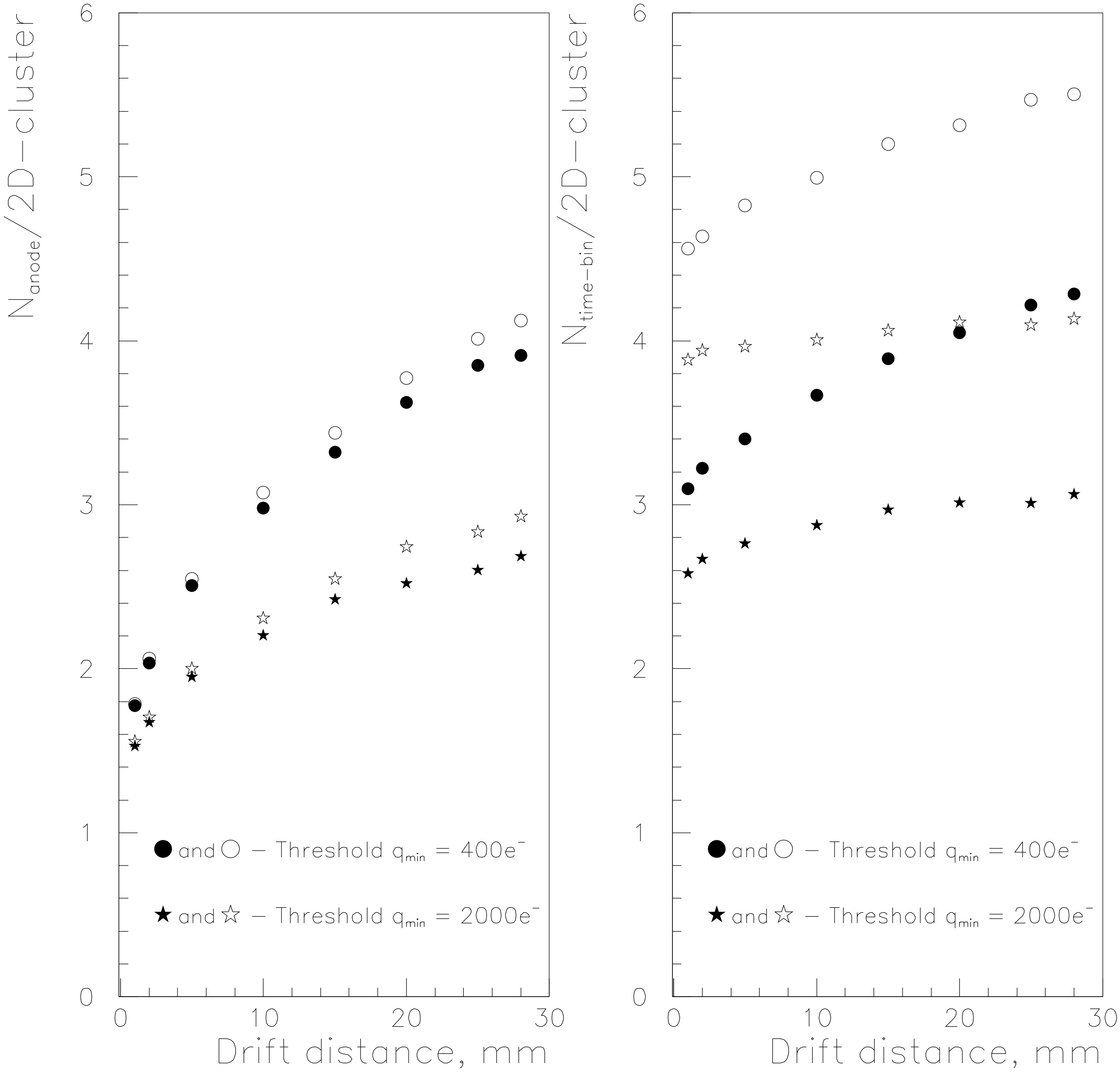

Figure 5: Mean 2D-cluster widths along the anode and drift axes vs drift distance. MIP, perpendicular hit, no noise. Solid markers correspond to PASA$_{short}$, open markers correspond to PASA$_{long}$.

provide information about the electron cloud size upon its arrival to the anodes and its alignment relative to the SDD "natural" frame of reference. The electron cloud widths in the principal axes frame of the cloud, w_{max} and w_{min}, can be derived using the formula:

$$w^2_{max/min} = \frac{1}{2}(m_{11} + \mu_{22}) \pm \frac{1}{2}\sqrt{(m_{11} - \mu_{22})^2 + 4m_{12}^2} \ , \quad (3)$$

where $\mu_{22} = m_{22} - \vartheta_M(X, Q, \ldots)$ is the estimate for the electron cloud width squared along the drift axis. The function $\vartheta_M(X, Q, \ldots)$ reflects the difference, originating from the PASA contribution, between the signal "drift-width", $\sqrt{m_{22}}$, and the width of the electron cloud, $\sqrt{\mu_{22}}$, along the drift axis. For a unipolar shaping function and fine signal sampling in both directions compared to the signal/cloud width, the difference ϑ_M should be a constant proportional to $(V_{drift} \cdot W_{pasa})^2$. In the real setup this is not the case, however. The practical way to obtain ϑ_M from simulations or calibrations is to "measure" the dependencies $< m_{11}(X, Q, \ldots) >$ and $< m_{22}(X, Q, \ldots) >$, averaged (notation $< \ldots >$) over many events of perpendicular particle crossings, where electron clouds are expected to be symmetric[4], i.e. $<m_{11}>=<\mu_{22}>$. Then the correction function can be derived as $\vartheta_M = < m_{22}(X, Q, \ldots) > - < m_{11}(X, Q, \ldots) >$. As soon as ϑ_M is known, it then can be used to estimate μ_{22} for each single hit, perpendicular or not.

The electron cloud tilt, i.e. the angle φ between its long principal axis and the drift direction, can be found using the equations:

$$\cos(2\varphi) = \frac{\mu_{22} - m_{11}}{\sqrt{(m_{11} - \mu_{22})^2 + 4m_{12}^2}} \ ; \quad \sin(2\varphi) = \frac{2m_{12}}{\sqrt{(m_{11} - \mu_{22})^2 + 4m_{12}^2}} \ . \quad (4)$$

5.2 2D-Gaussian fit

In the "2D-Gaussian fit" approach the signal distribution in the 2D-cluster is fit using by a two-dimensional, six-parameters Gaussian. One of its representational forms is the following:

$$u_{ij} \simeq \frac{Q_{2G}\, G_{pasa}\, W_{pasa}\, V_{drift}\, \Delta_z}{2.355\, \sqrt{2\pi}\, s_z\, s_x} \exp(-\frac{(Z_i - Z_{2G})^2}{2\, s_z^2} - \frac{(t_j \cdot V_{drift} - X_{2G} - \lambda Z_i)^2}{2\, s_x^2}) \ . \quad (5)$$

The free parameters are: the charge Q_{2G}, the centroid coordinates Z_{2G} and X_{2G}, and the three parameters, s_z, s_x and λ, relevant to the 2D-cluster/electron cloud size and its tilt. In terms of "Moment analysis", s_z^2 has the same meaning as m_{11}, the combination $s_x^2 + \lambda^2 s_z^2$ corresponds to m_{22}, and λs_z^2 corresponds to m_{12}. Using formulas (3) and (4), the same information as in the "Moment analysis" can be derived for the cloud size and its alignment. The drift-width correction function $\vartheta_{2G}(X, Q, \ldots)$ can be obtained in the same way as ϑ_M, but using a "2D-Gaussian fit" instead of the "Moment analysis".

5.3 1D-Gaussian fit

The "2D-Gaussian fit" can be used for 2D-clusters which consist of at least 6 pixels above the threshold and at least three rows in both the anode and drift directions. However, for a

[4]This assumption might not be correct in the case of an anisotropic electron cloud expansion due to, for example, non uniformity of the drift field.

considerable fraction of the hits, the cluster width along the anodes is not sufficient (see Fig. 5), while the size along the drift axis usually meets the minimum condition for a Gaussian fit. The two axes can be decoupled if information about the cloud alignment is not required.

The "1D-Gaussian fit" procedure is based on the assumption that the sums, $S_x(t_j) = \sum_i u_{ij}$ and $S_z(Z_i) = \sum_j u_{ij}$, can be approximated by Gaussians:

$$S_z(Z_i) \simeq \frac{Q_{1G}\, G_{pasa}\, W_{pasa}\, V_{drift}\, \Delta_z}{2.355\, w_z\, \Delta_x} \cdot \exp(-\frac{(Z_i - Z_{1G})^2}{2w_z^2}) \,, \tag{6}$$

$$S_x(t_j) \simeq \frac{Q_{1G}\, G_{pasa}\, W_{pasa}\, V_{drift}}{2.355\, w_x} \cdot \exp(-\frac{(t_j \cdot V_{drift} - X_{1G})^2}{2w_x^2}), \tag{7}$$

where Q_{1G}, Z_{1G}, X_{1G}, w_z and w_x are the parameters to be determined from the fit of expressions (6) and (7) to the measured $S_z(Z_i)$ and $S_x(t_j)$. Parameters Z_{1G} and X_{1G} are the estimates for the 2D-cluster center of gravity, i.e. for the position of the particle hit; $w_{z,x}$ are the cluster widths in the anode and drift directions; and Q_{1G} is the estimate for the collected charge.

5.4 Comparison

All three approaches to the reconstruction of the 2D-cluster parameters are compared in Fig. 6. Fig. 6a shows the "reconstruction efficiencies"[5] of one- and two-dimensional Gaussian fits for two PASA options and two thresholds q_{min} (the efficiency for the "1D-Gaussian fit" along the anode axis is not shown, but it is about the same as that for the "2D-Gaussian fit"). One can observe that the efficiencies are low for short drifts, in particular for the "2D-Gaussian fit". Therefore, for a fraction of the 2D-clusters, another algorithm with a higher applicability will have to be used, such as the "Moment analysis" which can be applied to clusters of any size.

In Fig. 6b–d, the "Moment analysis" and "Gaussian fits" are compared in terms of the charge and position resolutions[6]. Apparently, there are no sizeable differences between the resolutions provided by these three algorithms for most of the SDD. However, for short drifts, the "Moment analysis" gives noticeably better results for σ_x and $\Delta Q/Q$ due to its lower sensitivity to the signal shape. The simulations have shown that the same conclusions are true for other reasonable choices of the setup parameters. However, "Gaussian fits", compared to "Moment analysis", have two clear disadvantages: 1) low efficiency and 2) more complicated and time consuming calculations are required. Keeping these points in mind, throughout the remainder of this paper, the results of the simulations are usually shown for "Moment analysis" only.

[5] Here and throughout the rest of this paper the term "reconstruction efficiency" of the algorithm is a shortcut for the relative number of 2D-clusters which any particular algorithm can be applied to.

[6] The resolutions shown in Figs. 6–11, for any particular drift distance X, actually represent the numbers averaged over particle hits, uniformly distributed within a rectangle of the size $\Delta_z \cdot \Delta_x$; see Section 7 for details.

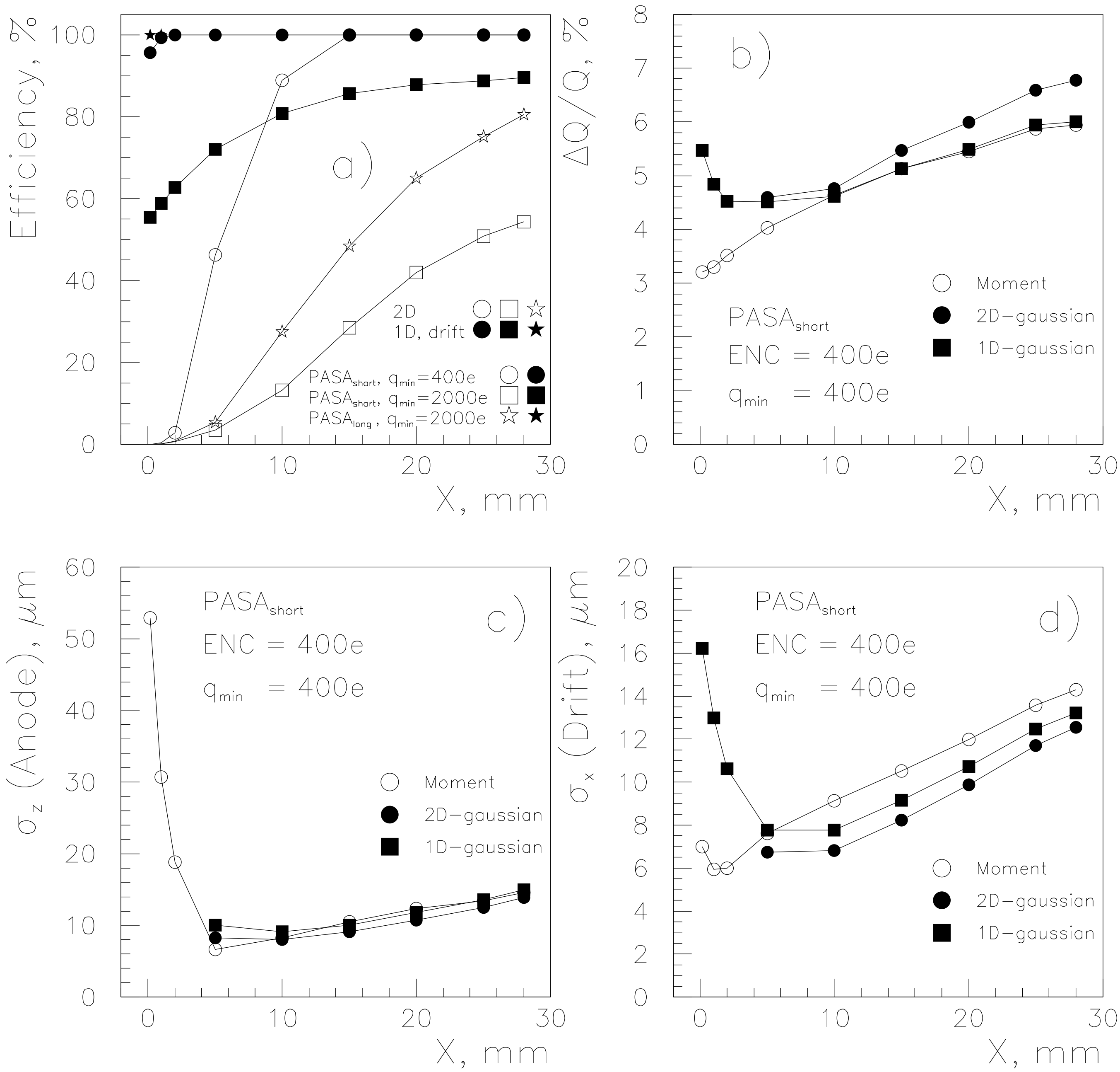

Figure 6: MIP, perpendicular crossings. Reconstruction efficiencies for "Gaussian fits", **a)**. Comparison of the charge, **b)**, and position resolutions, **c)** and **d)**, for "Moment analysis" and "Gaussian fits".

6 Position and charge resolutions

Figs. 7 presents SDD position resolution vs drift distance for two PASAs, various noise levels, and thresholds q_{min}. One can observe that, for the low noise and threshold, there are no significant differences between PASA$_{short}$ and PASA$_{long}$. However, for the higher noise and threshold, PASA$_{long}$ seems preferable. At the low noise level of $400e$, the expected position resolution for most of the SDD is within the limit of the SVT project goal of $\sim 25\,\mu m$, even with the high threshold $q_{min} = 5 \cdot ENC$. This is still true if the ENC is increased to $800e$ and the threshold to $q_{min} = 1 \cdot ENC$, but the resolution fails to meet the goal if q_{min} rises to $5 \cdot ENC$. This point can be interpreted as an indication that a noise level of $\sim 800e$ should be treated as the upper limit if the SVT is to meet its goal of a $25\,\mu m$ position resolution.

The achievable accuracy of the measurements of the ionization level and its dependence on the setup parameters is shown in Fig. 8. In general, one can expect the charge and, thus, the dE/dx resolution in a single SVT layer to be on the order of 5–10%.

A comparison of the position and charge resolutions for two different SCA readout frequencies and drift velocities is shown in Fig. 9. For the same drift velocity (SDD bias), a higher sampling rate gives a slightly better spatial resolution, particularly in the drift direction. However, an improvement in the range of only a few microns does not seem sufficient to justify doubling the SCA and the DAQ memory. At the slower drift, the charge resolution is degraded somewhat, while the position resolution is not affected significantly.

In the STAR experiment, particles will cross the SDD with a wide range of angles, up to 45–50^o, between the track and the normal vector to the SDD plane. The highest crossing angles are expected in the plane perpendicular to the drift direction ($r - z$ plane in the STAR frame of reference). The expected resolutions for non perpendicular tracks are shown in Fig. 10. The point to note here is that, for short drift distances and randomly distributed crossing angles, the average resolution in the anode direction is ~1.5 times better than the resolution for perpendicular tracks.

The simulations did not show any sizeable differences between the resolutions with correlated and uncorrelated noise (it may make a significant difference in a zero-suppression/cluster-finder algorithm, however). The 10-bit signal digitization and the limitation of the dynamic range of 2–2.1 V do not affect the resolutions for MIPs either. The dynamic range limit starts to play a negative role at higher ionization. Examples of such effects are shown in Fig. 11 for the ionization $Q_{track} = 750,000e$. The dynamic range limitation worsens the resolution for short drifts, but its contribution diminishes as the drift distance increases.

7 Corrections, calibration and overall SDD performance

The resolutions σ_z, σ_x, and ΔQ discussed above need to be commented upon further. The quantities plotted in Figs. 6–11 for any particular drift distance X represent values averaged over the sample of simulated particle hits which were uniformly distributed within the rectangle:

$$Z - \Delta_z/2 \leq Z_{track} \leq Z + \Delta_z/2\ , \quad X - \Delta_x/2 \leq X_{track} \leq X + \Delta_x/2, \tag{8}$$

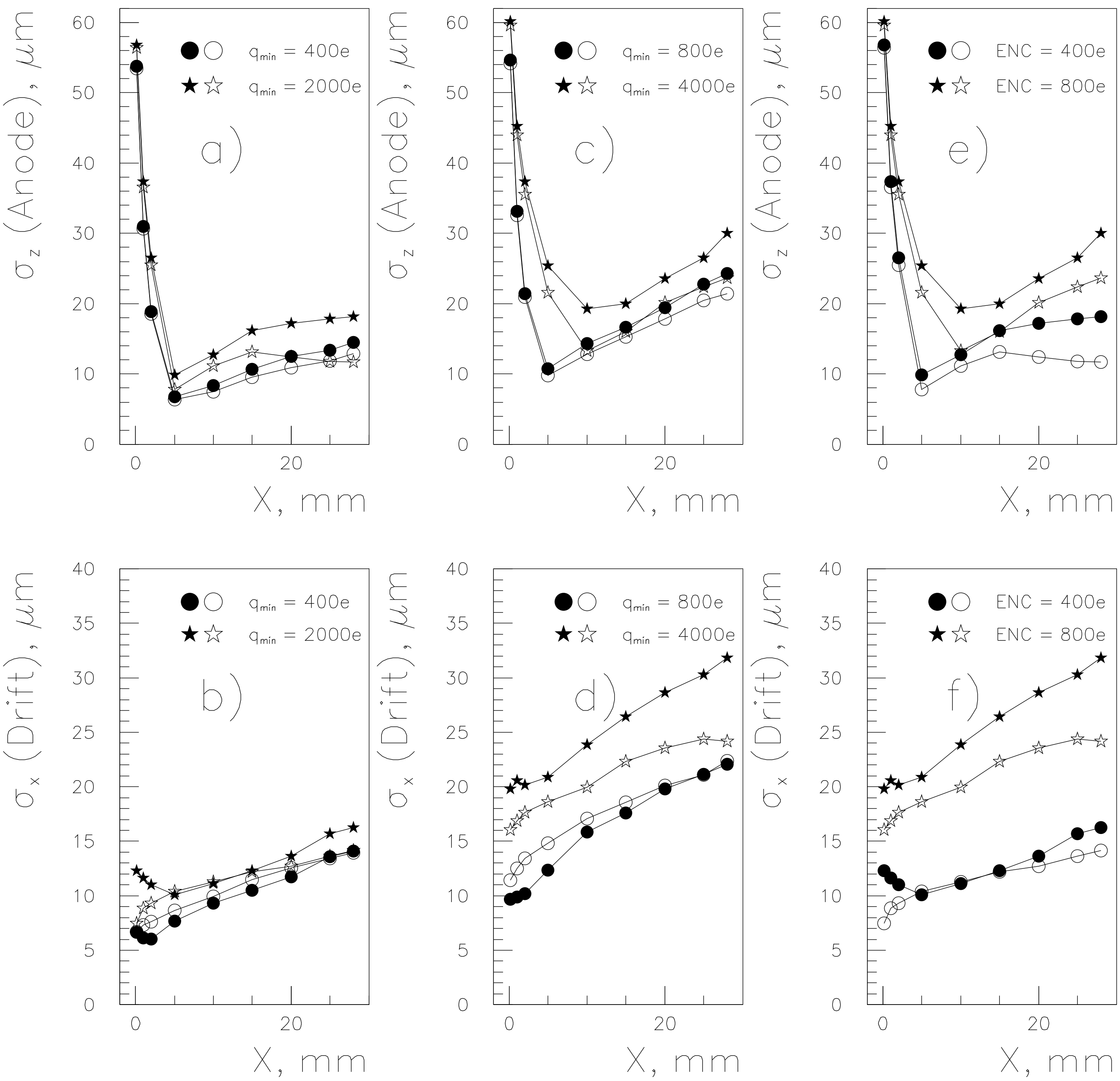

Figure 7: SDD position resolution vs drift distance X. MIP, perpendicular hits. Solid markers correspond to PASA$_{short}$, open markers correspond to PASA$_{long}$. **a)** and **b)** are for $ENC = 400e$; **c)** and **d)** are for $ENC = 800e$; **e)** and **f)** are the comparison of $ENC = 400$ and $800e$ with the threshold $q_{min} = 5 \cdot ENC$.

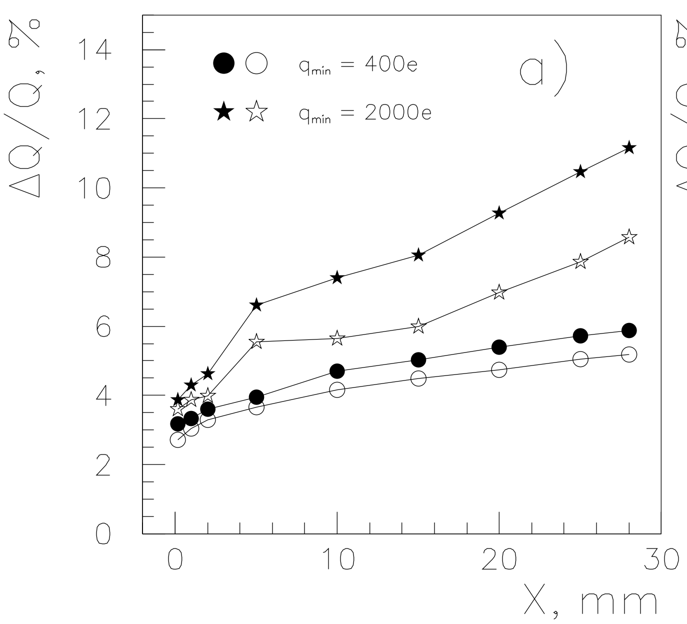

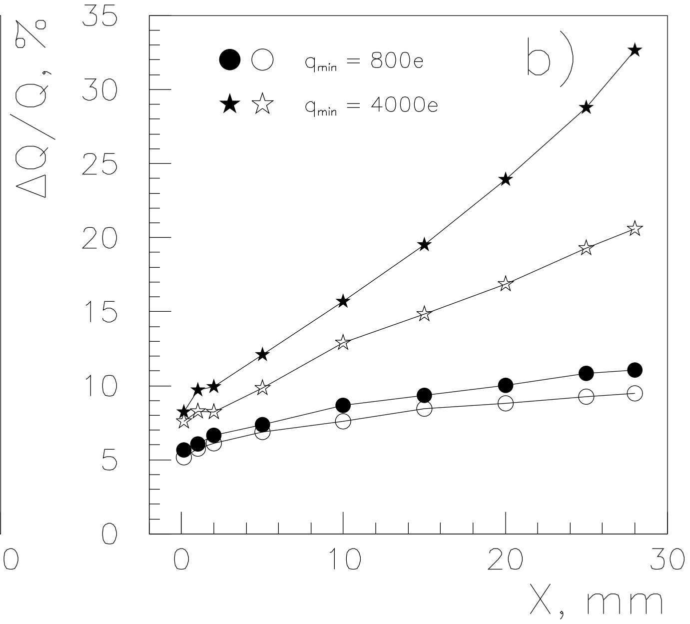

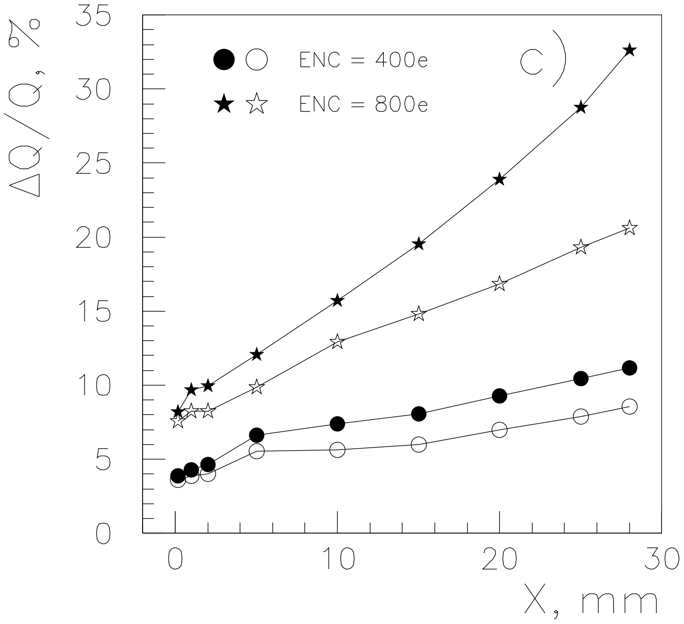

Figure 8: SDD charge resolution vs drift distance X. MIP, perpendicular hits. Solid markers correspond to PASA$_{short}$, open markers correspond to PASA$_{long}$. **a)** is for $ENC = 400e$; **b)** is for $ENC = 800e$; **c)** is the comparison of $ENC = 400$ and $800e$ with the threshold $q_{min} = 5 \cdot ENC$.

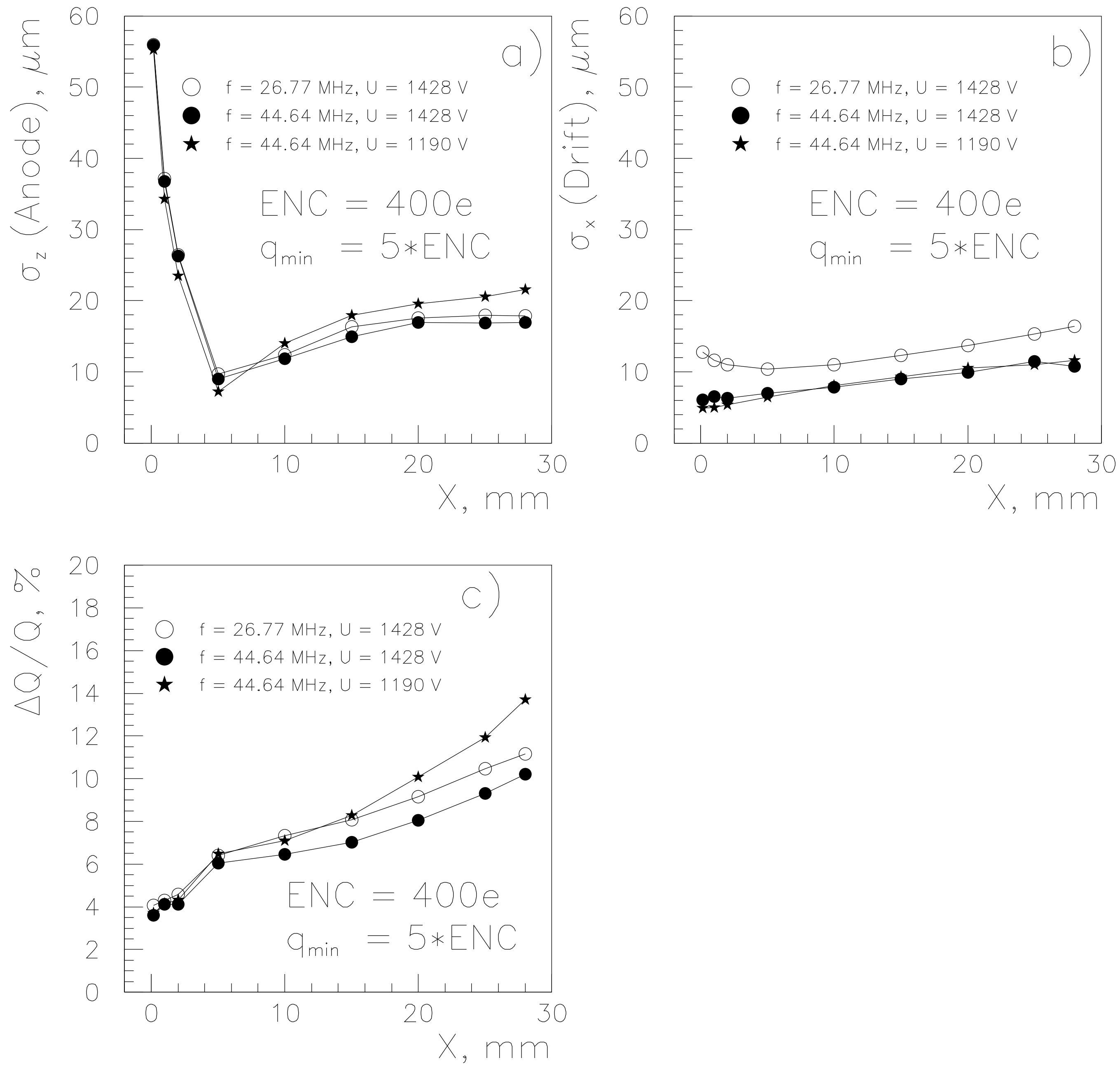

Figure 9: Comparison the position and charge resolutions for two values of the SCA readout frequency: $f_{SCA} = 26.7700$ and $44.6429\,MHz$. At the high frequency, the total number of time slices for the full drift length, $30\,mm$, is 214 and 256 for SDD biases of $U = 1428$ and $1190\,V$ respectively. MIP, perpendicular hits, PASA$_{short}$.

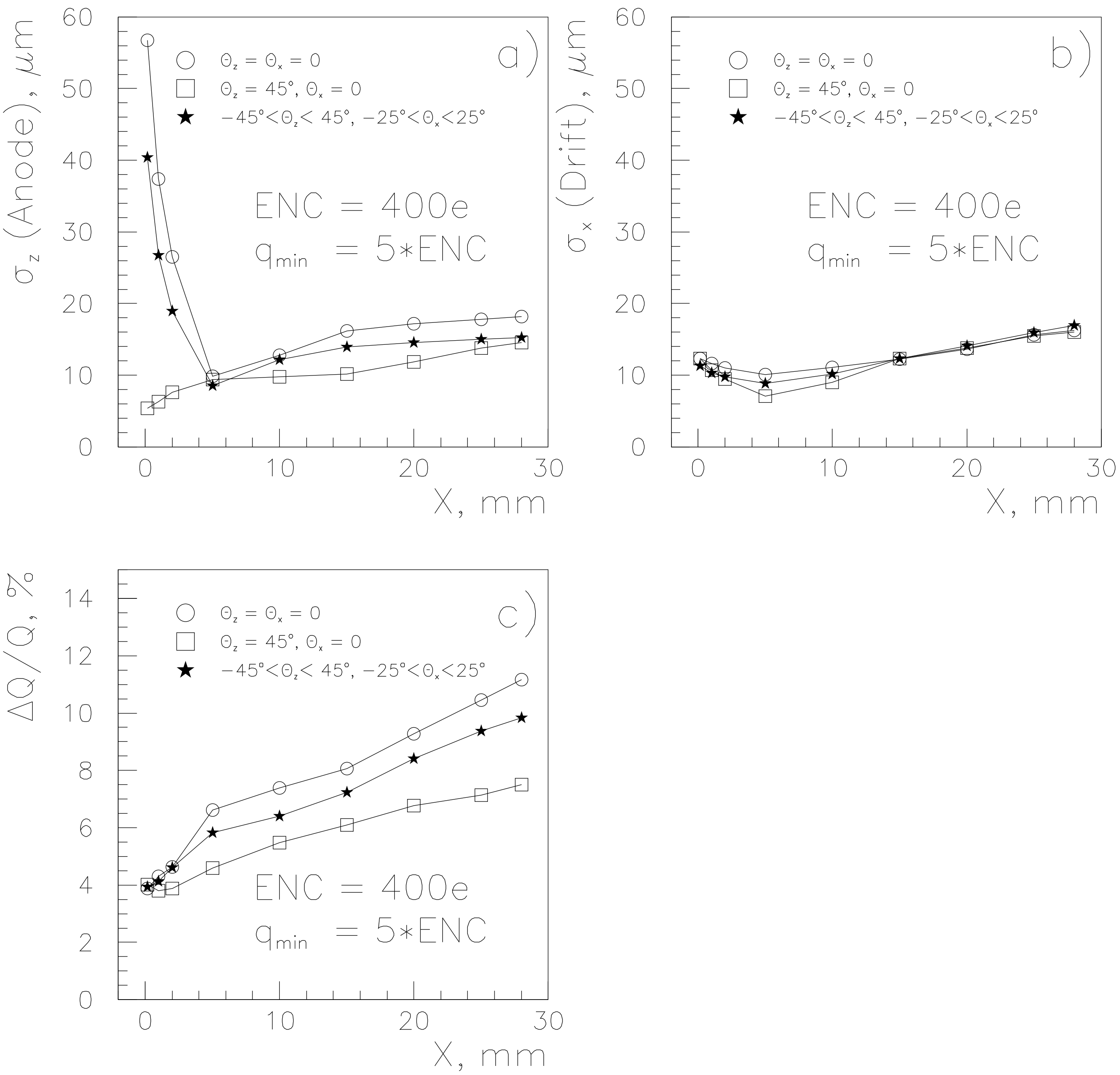

Figure 10: Position and charge resolutions for tracks crossing an SDD at various angles. Θ_z is the angle between the SDD normal vector and the projection of the particle trajectory onto the plane perpendicular to the drift axis; Θ_x is the angle between the SDD normal vector and the projection of the track onto the plane perpendicular to the anode axis. The notation $\Theta_{min} < \Theta_{z,x} < \Theta_{max}$ means that the tracks were uniformly distributed from Θ_{min} to Θ_{max}. MIP, PASA$_{short}$.

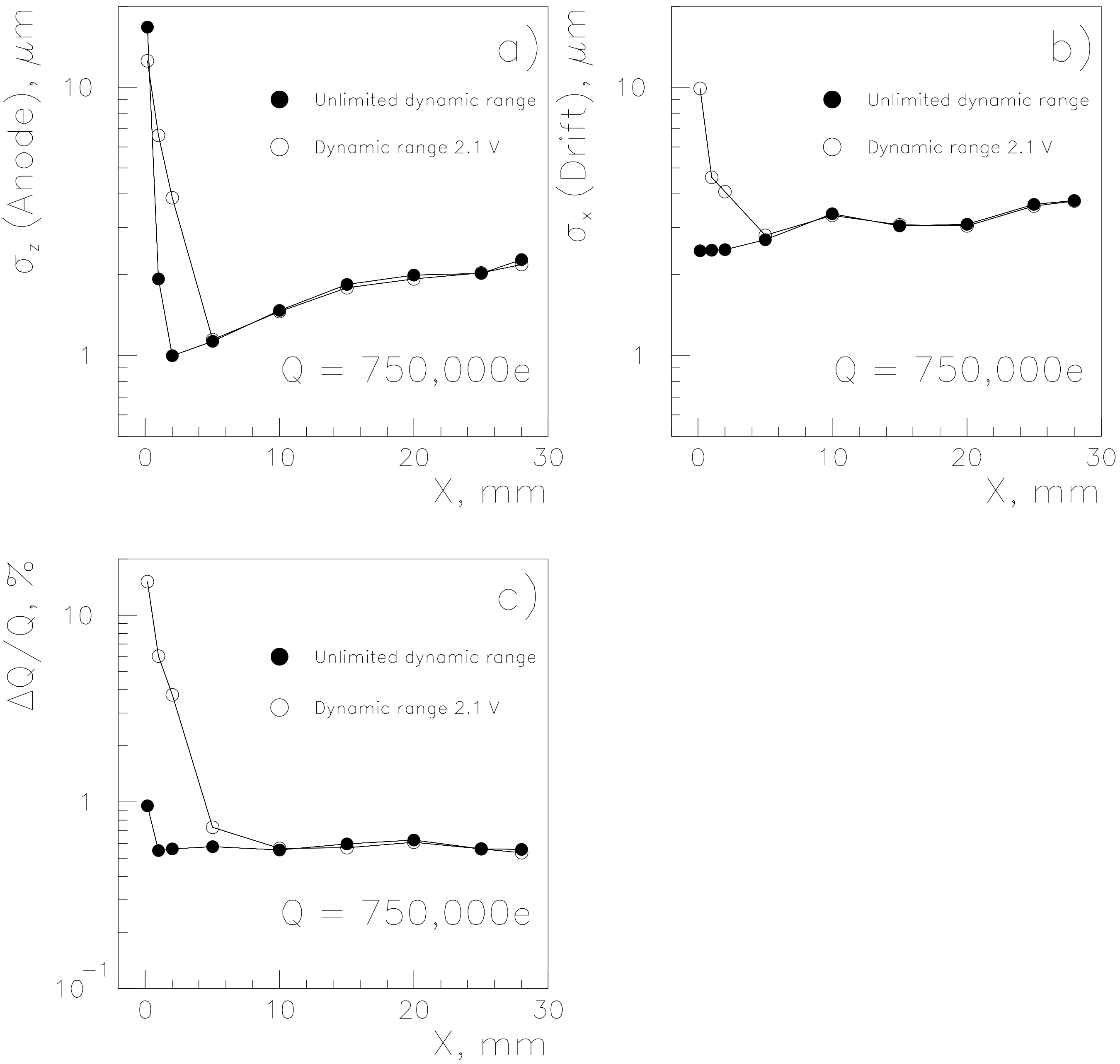

Figure 11: Position and charge resolutions for an ionization of $750,000e$ ("slow proton") with and without the dynamic range limitation. PASA$_{short}$, $ENC = 400e$, $q_{min} = 5 \cdot ENC$, $\mid \Theta_x \mid < 25^o$, $\mid \Theta_z \mid < 45^o$.

where Z is any coordinate within the SDD; Z_{track} and X_{track} are the crossing coordinates of a generated single particle track. The resolution along the anodes is defined as

$$\sigma_z(X) = \sqrt{< (Z_{M,G} - Z_{track})^2 >} = \sqrt{\frac{\sum_{track}(Z_{M,G} - Z_{track})^2}{N_{track}}} \ , \tag{9}$$

where N_{track} is the number of simulated hits, and $Z_{M,G}$ is the reconstructed position of the hit using either the "Moment analysis" (Z_M) or the "Gaussian fits" (Z_G) techniques.

In the drift direction, the definition of σ_x looks slightly different because, for $X_{M,G}$ from equations (2), (5) and (7), the mean value $< X_{M,G} - X_{track} >$ is not zero. At first glance, it would be expected to be a constant, close to the product $V_{drift} \cdot t_{peak}$. Therefore, the following expression should be used for σ_x estimations:

$$\sigma_x(X) = \sqrt{< (X_{M,G} - X_{track})^2 > -(< X_{M,G} - X_{track} >)^2} \ . \tag{10}$$

The real situation is even more complex due to the signal shape dependence on the drift distance, the ionization level, and the track crossing angle. The result is that the mean value $\Delta X =< X_{M,G} - X_{track} - V_{drift} \cdot t_{peak} >$ actually is not a "constant" close to zero, but rather a function of the signal time-width[7] which, in turn, is a function of the hit characteristics listed above. ΔX may also depend on the 2D-cluster definition and some other factors. Moreover, different reconstruction procedures may produce different functional dependencies $\Delta X(X, Q, \ldots)$.

The results of the simulations with MIPs, shown in Fig. 12a, illustrate this. Apparently, for PASA$_{short}$ there is no big difference between the three reconstruction algorithms. However, this is not the case for PASA$_{long}$ where $\Delta X_M(X)$ and $\Delta X_G(X)$ differ significantly. Therefore, if the SDD had been calibrated using any of these three reconstruction procedure, but then the analysis has been switched to another one, the resulting systematic errors in the position resolution may be as large as ~25–30 μm.

The ratio of the reconstructed charges $Q_{M,G}$ to the original ionization Q_{track}, which is shown in Fig. 12b, also exposes its dependence on the drift distance, the signal shaping, and the reconstruction algorithm used. Taking this into account, the value $\Delta Q/Q$ in the figures throughout the paper has been calculated using the formula:

$$\Delta Q/Q = \frac{\sqrt{< (Q_{M,G}/Q_{track})^2 > -(< Q_{M,G}/Q_{track} >)^2}}{< Q_{M,G}/Q_{track} >} \ . \tag{11}$$

The corrections to the drift position and the charge depend quite strongly on the ionization level (Figs. 12c,d), thus providing one more subject for the attention in the SDD calibrations. However, the good news is that neither $\Delta X_{M,G}$ nor $< Q_{M,G}/Q_{track} >$ show significant dependencies on the track crossing angles within the expected limits of their variations.

Fig. 13 presents the distributions averaged over entire SDD area with all corrections discussed above. These pictures confirm that the current SVT design is consistent with its ultimate goal for achieving a position resolution of $\leq$25 μm.

[7]The primary cause of the centroid position dependence on the signal width is the bipolarity of the PASA shaping function $f_{pasa}(t)$.

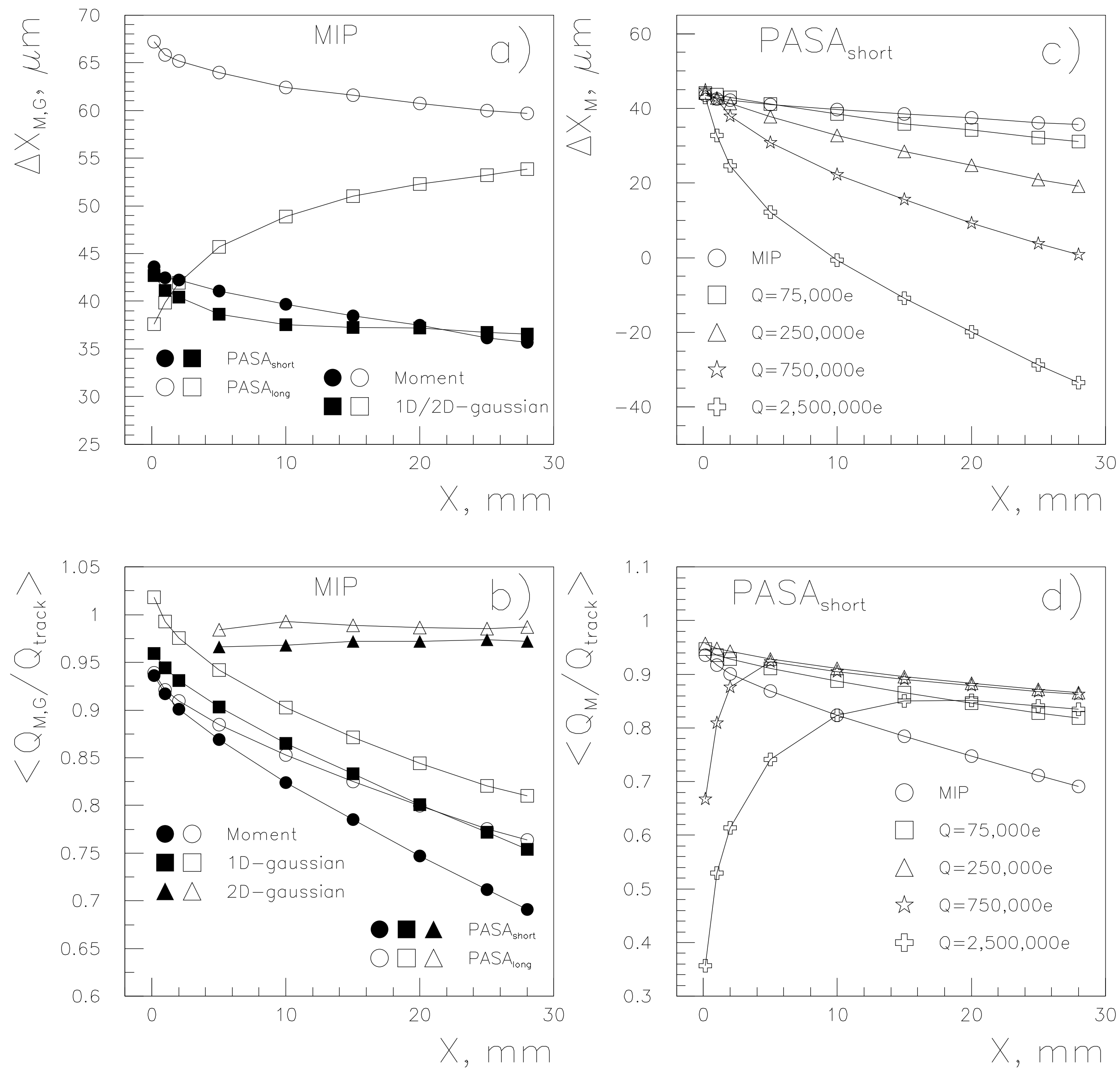

Figure 12: The corrections to the reconstructed drift position, ΔX, and charge, $<Q/Q_{track}>$, due to the variations of the signal shape; **a)** and **b)** are for MIP; **c)** and **d)** are for higher ionizations ("Moment analysis" only). $ENC = 400e$, $q_{min} = 5 \cdot ENC$. The effective dynamic range for the signals is 2.1 V; $\mid \Theta_x \mid < 25^o$, $\mid \Theta_z \mid < 45^o$.

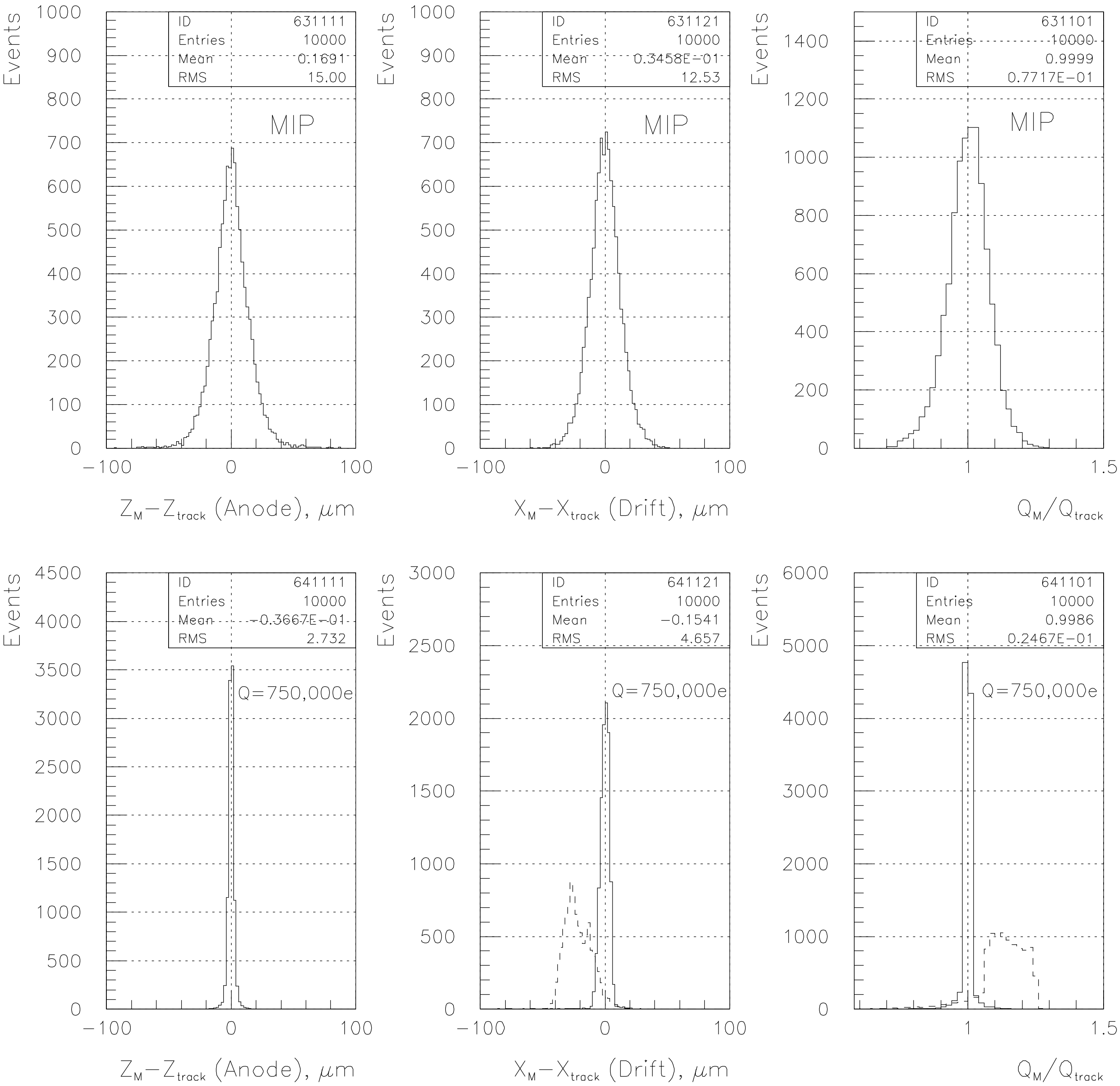

Figure 13: Position and charge resolutions over the entire SDD. The top row is for MIP; the bottom row is for $Q = 750,000e$. The dashed distributions for high ionization are obtained using ΔX and $< Q_M/Q_{track} >$ calibrations for MIP (HBOOK statistics are for the solid histograms). PASA$_{short}$, $ENC = 400e$, $q_{min} = 5 \cdot ENC$, dynamic range is 2.1 V, $\mid \Theta_x \mid < 25^o$, $\mid \Theta_z \mid < 45^o$.

8 Cluster size and alignment

The cluster size and its alignment can provide some criteria for the separation of real particle hits from false clusters, from clusters having the wrong timing, and recognition of overlapping multiparticle hits. The search for the corresponding criteria and the determination of their selection power is a subject for a special study and, eventually, for the detector calibration. Here just one example is discussed of what could be done, presumably at the software trigger level, using "Moment analysis".

Fig. 14 presents the event distributions in the "$w_{max} - X$" plane (maximum cloud size vs drift distance) for single and double particle (equal ionization) hits 300 μm apart with the same total charges $Q = 50,000e$. One can observe that the bands of the single and double hits are well separated for most of the total drift distance. At the statistical level of 10,000 hits, the w_{max}-distributions for perpendicular crossing at the mid-SDD do not overlap at all. The bottom row of pictures illustrates the accuracy of the reconstruction of the angle between the drift axis and the line connecting two hits in the cluster. The reconstruction errors are $\sim$6–7^o. These errors are almost independent of the PASA shaping time, but are slightly higher for non perpendicular tracks.

For the equal noise levels, the simulations do not show a considerable difference between PASA$_{long}$ and PASA$_{short}$ in double-hit recognition (it seems that, at the long drifts, the separation with PASA$_{long}$ is slightly better, though). A difference may become apparent when reconstructing double-hit parameters. This problem, however, along with the detailed study of the separation power of various criteria (cloud asymmetry w^2_{max}–w^2_{min}; χ^2 for various fits; etc) is the subject for a special investigation.

9 Conclusion

The results of the simulations presented in this papers confirm that the current SDD design, with the baseline version of PASA$_{short}$ and an integrated noise of $\leq$400e, meets the main SVT project goal for achieving a position resolution of $\leq$25 μm. Increasing the PASA shaping time by a factor of $\sim$1.5 while keeping the same noise level may give some further improvement in the position resolution and also in multiple hit recognition for long drifts. However, this point has to be studied more in regard to double hit parameter reconstruction as well as its connection to design issues.

The SCA readout frequency of 26.77 MHz with 128 time samples for the full drift length does not lead to a notable degradation of the resolution compared to higher sampling rates.

It has been shown that "Gaussian fits", when compared to "Moment analysis", usually do not noticeably improve the estimations of the particle hit parameters. However, the "Gaussian fits" approach has a number of disadvantages, namely, the low efficiency and the more complex and time consuming calculations.

A proper SDD calibration is vitally important for achieving the maximum performance the detector is able to provide. Full scale calibrations might be quite time consuming and not so trivial because of the non scalable signal shape dependence on many parameters (charge, drift distance, analysis procedure, etc). Eventually some sort of compromise can be worked out between the calibration complexity and the SVT performance, keeping the last within

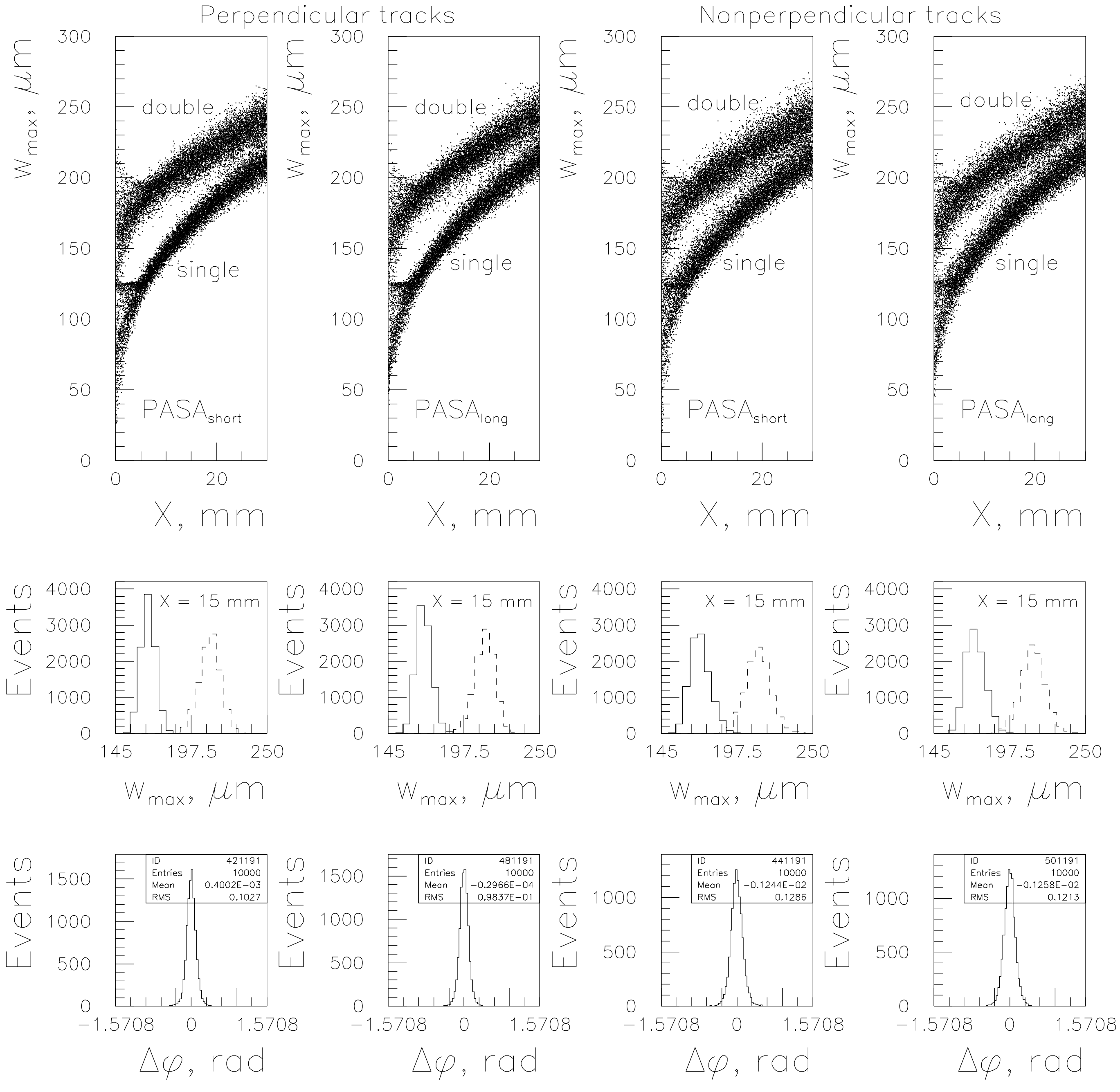

Figure 14: Top row: plots of the reconstructed maximum of the electron cloud size, w_{max}, for single and double particle hits 300 μm apart. Middle row: the cross-sections of the corresponding plots on the top at $X = 15$ mm (solid lines are for single hits, dashed lines are for double hits). Bottom row: the reconstruction accuracy of the relative alignment of two hits in the double clusters, averaged over the entire SDD (see text for details). MIP, PASA$_{short}$, $ENC = 400e$, $q_{min} = 1{\cdot}ENC$; for non perpendicular hits $\mid \Theta_x \mid < 25^o$, $\mid \Theta_z \mid < 45^o$.

the limits of the project goals.

Other, more specific requirements may result from the double particle reconstruction and zero-suppression/cluster-finder algorithms studies which are yet to be accomplished.

10 Acknowledgments

I'm pleased to thank my colleagues in the WSU Nuclear Science Group, R. Bellwied, T. M. Cormier, J. R. Hall, C. A. Pruneau, and W. K. Wilson, for the support of this research and useful discussions. The permanent and very helpful contacts to D. DiMassimo, D. Lynn, I. Kotov and J. Murgatroyd are also appreciated, as well as the efforts of C. Pruneau and D. Read in implementing the *SDD_SIGNAL* and *CORR_NOISE* codes in TAS.

References

[1] E. Gatti and P. Rehak, NIM **A289** (1990) 410.

[2] Conceptual Design Report for the Solenoidal Tracker at RHIC (The STAR Collaboration), BNL, June 15, 1992.

[3] V. L. Rykov, File: /ua2/rykov/star.dir/svt.dir/signal.dir/sdd_signal.f at RHIC computers in BNL, and the "User Guide" therein.

[4] V. L. Rykov and W. K. Wilson, Reports to the STAR Collaboration Meetings, August 1994 (BNL) and January 1995 (LBL).

[5] R. Bellwied, et al., Development of Large Linear Silicon Drift Detectors for STAR Experiment at RHIC. Report to the 7th European Symposium on Semiconductor Detectors. Munich, Germany, May 1995.

[6] D. DiMassimo, Private communications.

[7] D. Lynn, Private communications.

[8] V. L. Rykov, File: /ua2/rykov/mylib.dir/source.dir/corr_noise.f at RHIC computers in BNL, and the "User Guide" therein.

[9] J. F. Bak, et al, NIM, **B288** (1987) 681–716.

[10] STAR SVT Requirement Documents, August 1995.